OPEN

Correspondence and
requests for materials
should be addressed to
M.A. (mzan@hit.edu.
cn)

Superior cycle performance and high reversible capacity of SnO$_2$/graphene composite as an anode material for lithium-ion batteries

Lilai Liu[1,2], Maozhong An[1], Peixia Yang[1] & Jinqiu Zhang[1]

[1]State Key Laboratory of Urban Water Resource and Environment, School of Chemical Engineering and Technology, Harbin Institute of Technology, Harbin 150001, China, [2]College of Environmental and Chemical Engineering, Heilongjiang University of Science and Technology, Harbin 150022, China.

SnO$_2$/graphene composite with superior cycle performance and high reversible capacity was prepared by a one-step microwave-hydrothermal method using a microwave reaction system. The SnO$_2$/graphene composite was characterized by X-ray diffraction, thermogravimetric analysis, Fourier-transform infrared spectroscopy, Raman spectroscopy, scanning electron microscope, X-ray photoelectron spectroscopy, transmission electron microscopy and high resolution transmission electron microscopy. The size of SnO$_2$ grains deposited on graphene sheets is less than 3.5 nm. The SnO$_2$/graphene composite exhibits high capacity and excellent electrochemical performance in lithium-ion batteries. The first discharge and charge capacities at a current density of 100 mA g^{-1} are 2213 and 1402 mA h g^{-1} with coulomb efficiencies of 63.35%. The discharge specific capacities remains 1359, 1228, 1090 and 1005 mA h g^{-1} after 100 cycles at current densities of 100, 300, 500 and 700 mA g^{-1}, respectively. Even at a high current density of 1000 mA g^{-1}, the first discharge and charge capacities are 1502 and 876 mA h g^{-1}, and the discharge specific capacities remains 1057 and 677 mA h g^{-1} after 420 and 1000 cycles, respectively. The SnO$_2$/graphene composite demonstrates a stable cycle performance and high reversible capacity for lithium storage.

L ithium-ion batteries (LIBs), as power sources for portable electronic devices, mobile communication devices and electric/hybrid vehicles, have attracted tremendous attention due to their high energy density, high working voltage and excellent cycle life. Graphite is the most widely used commercial anode material. However, with a theoretical specific capacity of 372 mA h g^{-1}, graphite cannot meet the increasing demand for high capacity batteries. Therefore, the development of new alternative anode materials with higher performance is desired. Graphene, a one-atom-thick planar sheet of sp^2-bonded carbon with a theoretical lithium storage capacity of 744 mA h g^{-1}, has been widely studied for potential application in LIBs because of its unique properties, such as superior electronic conductivity, high theoretical specific surface area exceeding 2600 m^2 g^{-1}, and excellent mechanical properties[1–2]. Recently, chemically modified graphene with high surface area has been an attractive choice for synthesizing hybrid nanomaterials with the aim of improving their capacities, examples including CuO/graphene, Cu$_2$O/graphene, CoO/graphenen, Co$_3$O$_4$/graphene, Fe$_2$O$_3$/graphene, Fe$_3$O$_4$/graphene, Mn$_3$O$_4$/graphene, NiO/graphene, SnO$_2$/graphene, TiO$_2$/graphene, VO$_2$/graphene, and V$_3$O$_7$ nanowire templated graphene scrolls[3–16]. When used as anode materials for LIBs, these composites exhibited excellent electrochemical performances. Graphene sheets with various nanoparticles were used as anode materials for LIBs, which not only enhanced the unique properties of graphene and nanoparticles but also added novel functionality and properties due to the interaction between the materials. Graphene sheets could buffer the volume changes of nanoparticles and prevent them from conglomerating. Conversely, the nanoparticles can avert stacking of graphene sheets. SnO$_2$ is considered as one of the most promising anode material substitutes due to its high theoretical specific capacity (782 mA h g^{-1}) and low potential for lithium alloying[17–21]. Therefore, much research of SnO$_2$/graphene composites used as an anode material has been conducted. Various approaches to fabrication of SnO$_2$/graphene composites were reported, such as gas-liquid interfacial reaction, co-precipitation, in situ chemical synthesis, in situ oxidation route, hydrothermal, laser irradiation, microwave and ultrasonication methods[22–25]. Lian et al.[14] prepared a SnO$_2$/graphene composite by a gas-liquid interface reaction that exhibited a
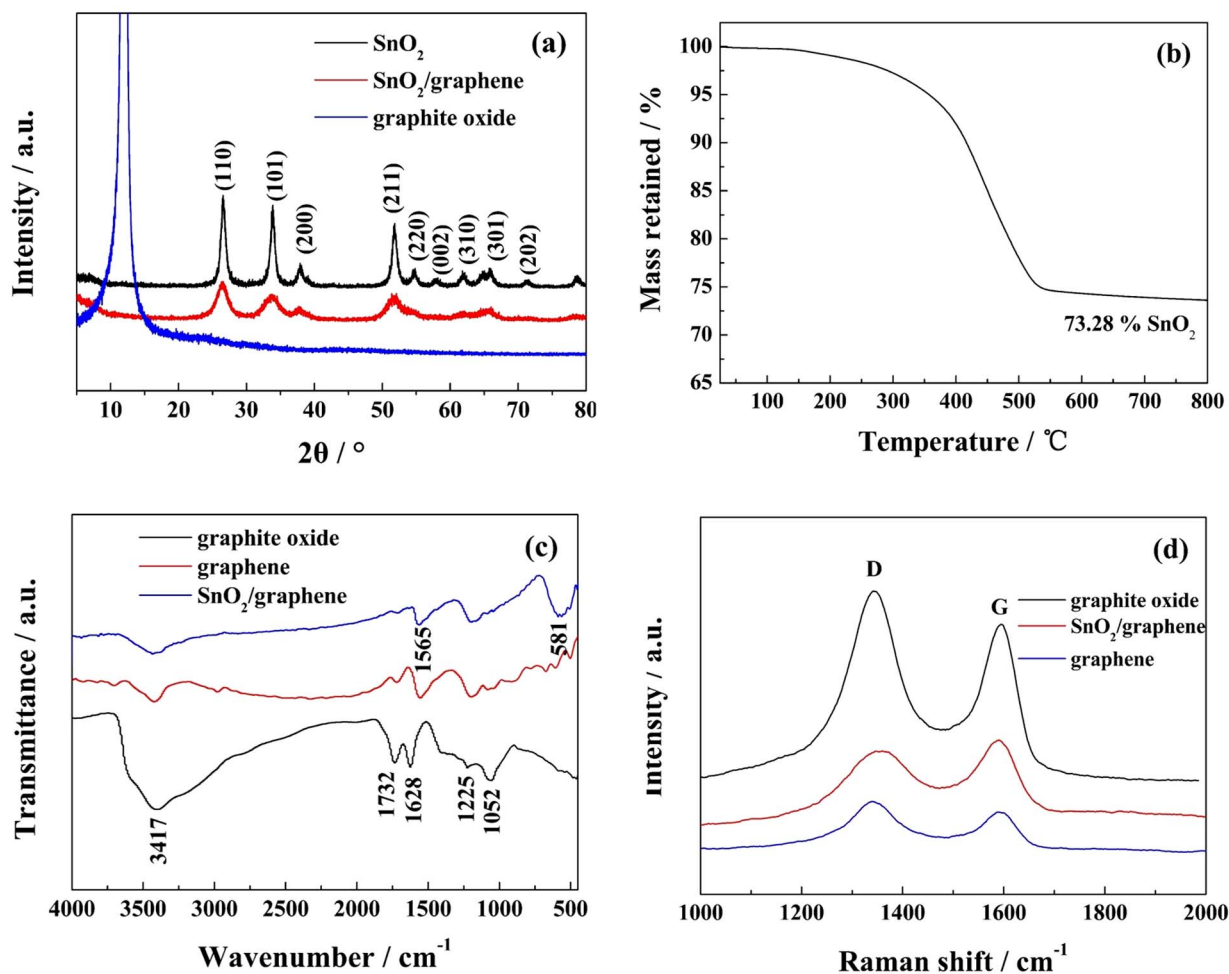
Figure 1 | Structures of samples. (a) XRD patterns of SnO₂, graphite oxide and SnO₂/graphene, TGA curve of SnO₂/graphene composite measured in air atmosphere with a heating rate of 20°C min⁻¹, (c) FT-IR spectra and (d) Raman spectra of graphite oxide, graphene and SnO₂/graphene.

high reversible specific capacity when used as an anode material for LIBs. Zhao *et al.*[22] introduced a graphene/SnO₂ composite by the bivalent tin ion-assisted reduction method. Electrochemical measurement results showed that the composite could deliver a reversible capacity of 775.3 mA h g⁻¹ and capacity retention of 98% after 50 cycles. Zhu *et al.*[23] reported that a reduced graphene/tin oxide composite was synthesized by homogeneous co-precipitation and had capacities of 2140 and 1080 mA h g⁻¹ at 100 mA g⁻¹ for the first discharge and charge, respectively. Moreover, the composite exhibited good capacity retention with 649 mA h g⁻¹ after 30 cycles. Yao *et al.*[16] synthesized by an in situ chemical synthesis approach a SnO₂/graphene composite with a reversible capacity of 765 mA h g⁻¹ for the first cycle. Recently, several varieties of graphene/SnO₂ nanoparticle composites have been reported as anode materials for LIBs, such as flower-like SnO₂, SnO₂ nanorods, SnO₂ hollow nanosphere composites, ternary hybrids of graphene/SnO₂/Au, SnO₂-graphene-carbon nanotube mixtures and graphene/carbon nanosphere composites[24–30]. These SnO₂/graphene hybrids used as anode for LIBs had different structures and exhibited excellent electrochemical performance. However, the cycling stability performance for LIBs at high current densities need to be improved. In addition, most of the preparation methods of these materials used dried neutral graphene oxide as a precursor material and required auxiliary reagents, which result in complex and time-consuming processes. Therefore, an easy and efficient method for synthesizing graphene/metal oxide composites with high capacity for LIBs should be developed.

In this study, we report a one-step microwave-hydrothermal method for the synthesis of SnO₂/graphene composite with a micro-wave reaction system. This method features are quick heating, easily controlled pressure and temperature, high yield rate, and good homogeneity. In reaction process, a precursor material of liquid graphene oxide is reduced in situ, and a bivalent tin ion is oxidized without auxiliary reagents. The uniform composite shows high specific capacity and excellent cycling stability performance for LIBs at high current densities.

Results

Microstructural characterization. The structures of materials were systematically research. The X-ray diffraction (XRD) patterns of the prepared products are illustrated in figure 1 (a). The diffraction peaks of crystalline SnO₂ nanoparticles are clearly distinguishable. All strong diffraction peaks are consistent with a tetragonal crystalline SnO₂ phase (JCPDS card no. 41–1445). No diffraction peaks of graphene and graphite oxide are observed in the SnO₂/graphene composite, indicating that graphite oxide is reduced to graphene and the graphene layer is exfoliated completely[14,25,31]. This observation helps support the inference that graphene oxide is reduced in situ by bivalent tin ions. For quantifying the content of SnO₂ in the SnO₂/graphene composite, thermogravimetric analysis (TGA) was carried out in air. The sample was heated from 25 to 800°C at a rate of 20°C min⁻¹. The TGA curve of the SnO₂/graphene composite is shown in figure 1 (b). From 250 to 550°C,the weight loss increases dramatically with the rise of temperature, attributed to the oxidation and decomposition of graphene. After 700°C,there is no obvious mass loss. From the result, we can approximately calculate
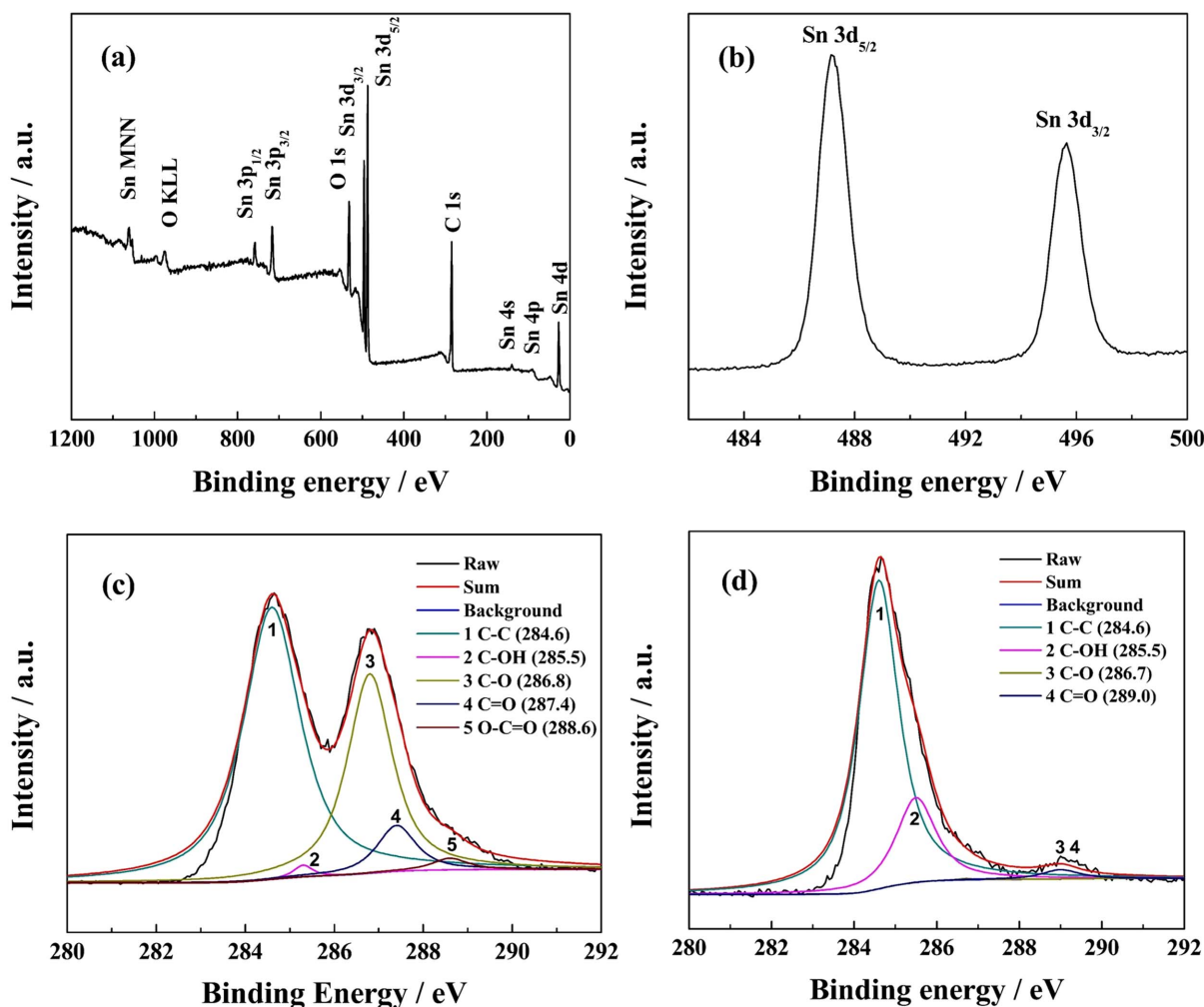
Figure 2 | XPS spectra of graphene and SnO$_2$/graphene. (a) general XPS spectrum of SnO$_2$/graphene, (b) Sn 3d XPS spectrum of SnO$_2$/graphene, (c) C 1s XPS spectra of graphite oxide and (d) C 1s XPS spectra of SnO$_2$/graphene.

the mass content of SnO$_2$ in the composite is 73.28%. The Fourier transform infrared (FT-IR) spectra of graphite oxide, graphene and SnO$_2$/graphene is presented in figure 1 (c). The peak at 3417 cm^{-1} can be attributed to O-H stretching vibrations of adsorbed water molecules and structural −OH groups. In the graphite oxide spectrum, the peak at 1628 cm^{-1} can be attributed to O-H bending vibrations. Carboxyl and epoxy functional groups can also be detected at approximately 1732, 1225, and 1052 cm^{-1}, respectively. Compares to the FT-IR spectrum of graphite oxide, those of graphene and SnO$_2$/graphene show that carboxyl group peaks at 1732 cm^{-1} decrease significantly, while carboxyl group peaks at 1225 cm^{-1} and those of epoxy functional groups at 1052 cm^{-1} disappeared. Two strong peaks of SnO$_2$/graphene are detected at 581 and 1565 cm^{-1} that corresponds to Sn-O-Sn antisymmetric vibrations and skeletal vibrations of the graphene sheets, respectively[32]. The Raman spectra of graphite oxide, graphene and SnO$_2$/graphene are shown in figure 1 (d). The peak at approximately 1581 cm^{-1} (G band) corresponds to the E$_{2g}$ mode of graphite, which is related to the vibration of sp^2-bonded carbon atoms in a 2-dimensional hexagonal lattice. The peak at approximately 1346 cm^{-1} (D band) is an indication of defects associated with vacancies, grain boundaries and amorphous carbon species[33]. Raman spectra with characteristic G and D bands are sensitive to defects, disorder and carbon grain size, and have been used extensively in the characterization of carbon materials. The intensity ratio (I_D/I_G) of the D band to the G band is related to the extent of disorder degree and average size of the sp^2 domains[34]. From figure 1 (d), the I_D/I_G of SnO$_2$/graphene is lower than those of graphite oxide and graphene sheets, indicating that bivalent tin can increase the order degree of graphene layers.

The surface chemistry of the SnO$_2$/graphene composite obtained from the X-ray photoelectron spectroscopy (XPS) is presented in figure 2. Figure 2 (a) shows the general XPS spectrum of SnO$_2$/graphene, which reveals the presence of carbon, oxygen and tin, and no other elements are detected. The peaks of Sn 3d, 4d, 3p, 4p and 4s from SnO$_2$ are observed. The peak of C 1s is attributed mainly to graphene. The Sn 3d spectrum, as shown in figure 2 (b), two peaks at 487.2 and 495.6 eV are attributable to Sn 3d$_{5/2}$ and Sn 3d$_{3/2}$ spin-orbit peaks of SnO$_2$, confirming the formation of SnO$_2$ nanoparticles on the surface of graphene sheets. Figure 2 (c) and (d) display the spectra of C 1s of graphite oxide and SnO$_2$/graphene. The C 1s region of graphite oxide gives five components at around 284.6, 285.5, 286.8, 287.4 and 288.6 eV, which can be generally assigned to the C-C, C-OH, C-O, C=O and O-C=O components, respectively[35]. In contrast, SnO$_2$/graphene exhibits dramatically decreased intensities of the C 1s components associated with carbon-oxygen bond, which indicates that most of the oxygenated functional groups on graphene oxide have been removed during the microwave-hydrothermal process. A few residual functional groups are reported to be useful in obtaining stable, highly dispersed SnO$_2$ particles[36].

The morphologies of graphite oxide, graphene sheets, SnO$_2$ and the SnO$_2$/graphene composite are observed by scanning electron
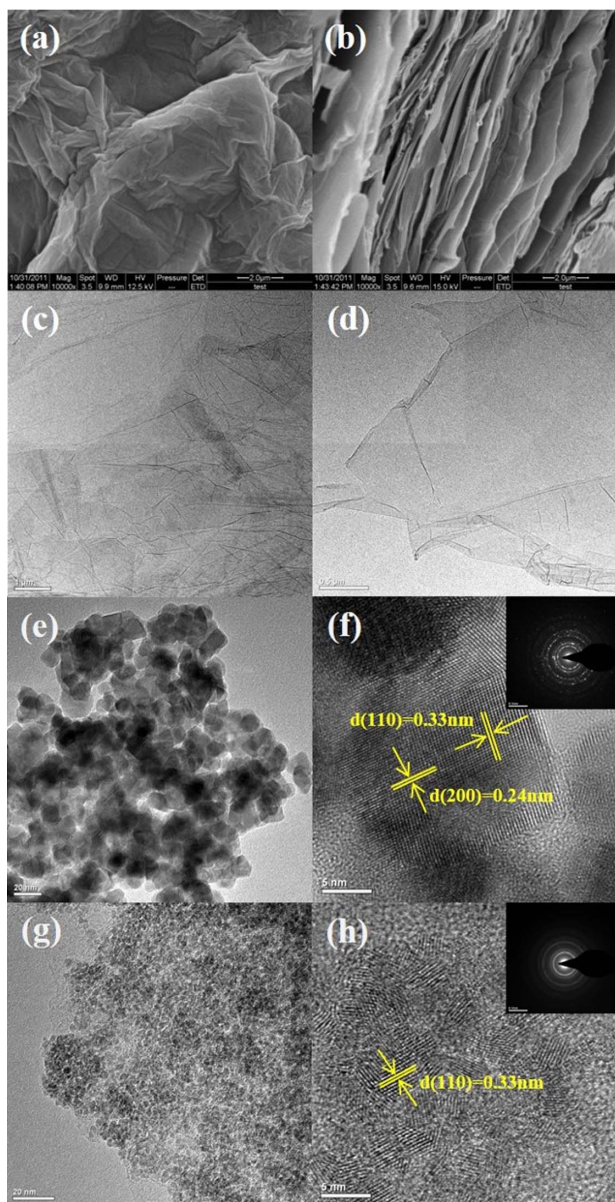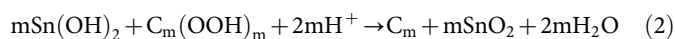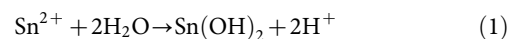
Figure 3 | Morphology characterization of graphite oxide, graphene, SnO₂ nanoparticles and SnO₂/graphene. (a)(b) SEM images of graphite oxide, (c) (d) TEM images of graphene sheets, (e) TEM images of SnO₂ nanoparticles, (f) High resolution transmission electron microscopy (HRTEM) images of SnO₂ nanoparticles, (g) TEM images of SnO₂/graphene, and (h) HRTEM of SnO₂/graphene.

microscope (SEM), transmission electron microscopy (TEM) and high resolution transmission electron microscopy (HRTEM). Figure 3 (a) and (b) present the SEM images of graphite oxide, showing the layered platelets are composed of curled and wrinkled graphene sheets. It is obvious that the graphene sheets are agglomerated and overlapped. Figure 3 (c) and (b) show TEM images of graphene sheets prepared using the one-step microwave-hydrothermal method. The larger graphene sheet is transparent and resembles a piece of gauze. From figure 3 (e), SnO₂ nanoparticles prepared using the microwave-hydrothermal method aggregated into large particles, and the average particle diameter of SnO₂ nanoparticles is 13 nm. These large particles can be pulverized easily owing to an asymmetric volume change during the Li₊ insertion/extraction process[37–38]. However, the TEM image of SnO₂/graphene in figure 3 (g) shows that the graphene sheets is covered by ultrafine SnO₂ nanoparticles and the diameter of the SnO₂ grains is less than

3.5 nm, indicating that the graphene sheets can prevent the SnO₂ nanoparticles from growing effectively. From the HRTEM images in figure 3 (f) and (h), the interplanar distances of 0.33 and 0.24 nm can be identified as d (110) and d (200) of SnO₂ nanoparticles, respectively. According to electron diffraction patterns (insets of figure 3 (f) and (h)), the four distinct diffraction rings represent (110), (101), (200), and (210) from the rutile phase of SnO₂, confirming the highly crystalline nature of SnO₂ nanoparticles[39–40].

According to the microstructural characterization results, a possible formation mechanism for the one-step microwave-hydrothermal reaction without using organic solvent or surfactant is described in the schematic representation of the fabrication process of SnO₂/graphene (figure 4) and the following equations:

$$Sn^{2+} + 2H_2O \rightarrow Sn(OH)_2 + 2H^+ \qquad (1)$$

$$mSn(OH)_2 + C_m(OOH)_m + 2mH^+ \rightarrow C_m + mSnO_2 + 2mH_2O \qquad (2)$$

The graphene oxide is prepared by modified Hummers method with the expanded graphite as a material. The larger layer spacing of expanded graphite can improve the efficiency of oxidation, the degree of oxidation and stripping of graphene oxide. There are plenty of oxygen containing functional groups on the surface and edge of graphene sheets. The bivalent tin ion underwent hydrolysis and rapidly transforms to $Sn(OH)_2$ with the assistance of microwave heating. Then $Sn(OH)_2$ is oxidized to SnO_2 by oxygen from the oxygenated functional groups of graphene oxide in the Teflon vessels at 200°C. The precursor liquid graphene oxide loses oxygen atoms and is reduced to graphene sheets in situ. In sealed high pressure Teflon vessels of the microwave reaction system, when microwave radiates graphene oxide and $SnCl_2 \cdot 2H_2O$ mixed solution, graphene oxide and water molecules transform their orientation quickly with the microwave frequency. At the same time, Sn^{2+} and hydrated ion of graphene oxide solution transfer back and forth, and strike with adjacent molecules under the function of electric field force. The total energy of the molecules is increased due to molecules rotate and collisions of friction. Therefore the solvent can be brought to a temperature well above its boiling point by the increase of pressure resulting from heating, which is beneficial to the rapid nucleation of nanoparticles. In addition, overheated supercritical water can also play the role of reducing agent and offers a green chemistry alternative to organic solvents during this reaction. The physiochemical properties of overheated supercritical water can be widely changed with changes in high pressure and high temperature, which allow the catalysis of a variety of heterolytic (ionic) bond cleavage reactions in water[41]. Under high temperature and pressure, the SnO₂ nanoparticles can distribute on graphene sheets uniformly and form nanoporous composite with a large number of void spaces. The large number of void spaces can buffer large volume changes of SnO₂ nanoparticles during the lithium ion insertion/extraction process[12,18,42]. The graphene sheets are distributed between the SnO₂ nanoparticles, preventing the aggregation of these nanoparticles to a certain extent[22–23]. Moreover, SnO₂ nanoparticles on the surface of graphene can also prevent the graphene from stacking into multilayers.

Electrochemical properties. In order to study the lithium storage performances and mechanism of electrode material, the LIBs of SnO₂/graphene composite as an anode material were tested. Figure 5 (a) shows the 1st, 2nd and 100th discharge and charge curves of SnO₂ and SnO₂/graphene at a current density of 100 mA g⁻¹ in the voltage range of 3.0 ~ 0.0 V vs. Li⁺/Li. In the first cycle, the discharge/charge capacities of SnO₂/graphene and SnO₂ are approximately 2213/1402 and 1607/833 mA h g⁻¹ with coulomb efficiencies of 66.74 and 51.84%, respectively. The initial small plateau in the potential range of 1.2 to 0.8 V corresponds to a classical conversion reaction between SnO₂ and Li⁺ and resulted in
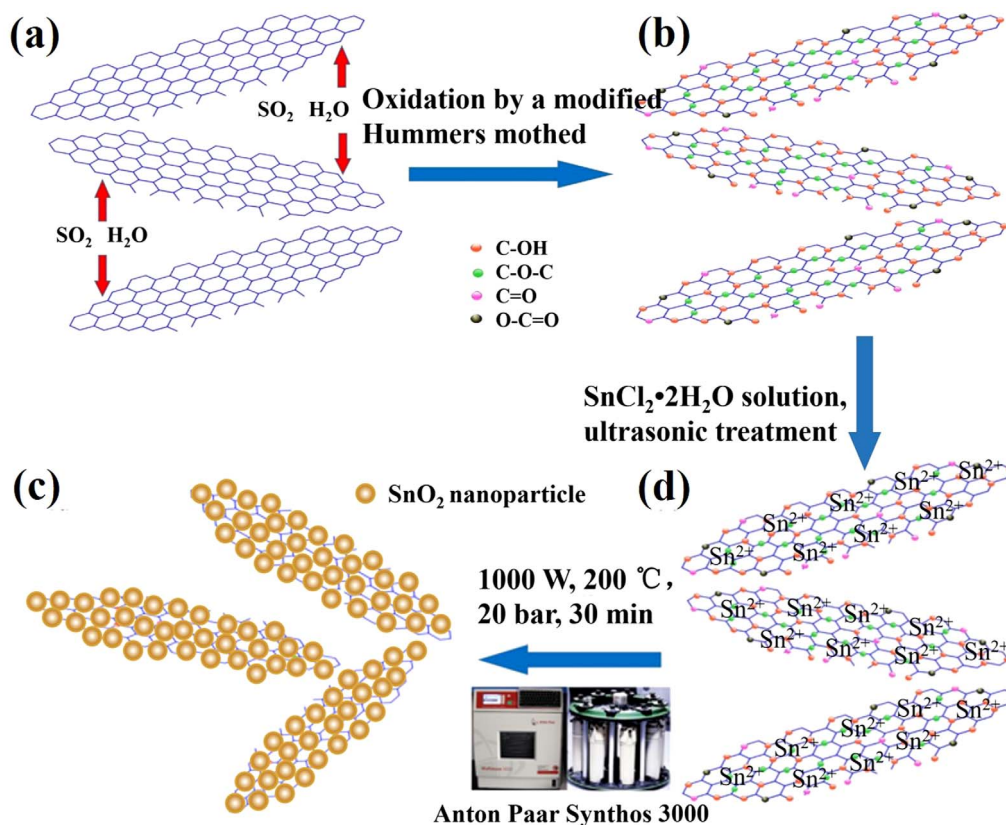
Figure 4 | Schematic representation of the fabrication process of SnO₂/graphene. (a) Expanded graphite, (b) Graphene oxide, (c) Graphene oxide and SnCl₂·2H₂O mixed solution and (d) SnO₂/graphene composite.

the formation of Sn and Li_2O in the first discharge of SnO_2/graphene, which corresponds to the cathodic peak at approximately 0.85 V. The plateau nearly disappeared during the second cycle, demonstrating that a large amount of Li_2O is formed during the first cycle. Because of this irreversible reaction, as well as the solid electrolyte interface (SEI) formed on the anodes[43–44], the discharge capacity dropped from 2213 to 1402 mA h g⁻¹, and the discharge capacity of SnO_2 dropped more significantly.

The Cyclic voltammetry (CV) curves of SnO_2/grapehen is shown in figure 5 (b). In the first cycle, two obvious cathodic peaks appeared around 0.85 and 0.02 V. The peak around 0.85 V is ascribed to the formation of SEI layers on the surface of the active materials, the reduction of SnO_2 to Sn, and the synchronous formation of Li_2O (Eq. (3))[11,14]. The peak at approximately 0.02 V corresponds to the formation of a series of Li_xSn alloys (Eq. (4))[23]. In the first anodic process, there is a small peak near 0.17 V, which can be attributed to Li intercalation into graphite to form LiC_6 (Eq. (5))[45]. There are also two obvious plateaus at 0.61 and 1.28 V, which can be ascribed to Li dealloying from Li_xSn and the partially reversible reaction from Sn to SnO_2, respectively. The CV measurements clearly elucidated the reversible electrochemical reactions between the lithium ions and the SnO_2/graphene composite in lithium ion cells. The reactions are described in the following equations:
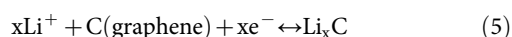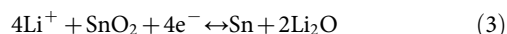
$$4Li^+ + SnO_2 + 4e^- \leftrightarrow Sn + 2Li_2O \qquad (3)$$

$$xLi^+ + Sn + xe^- \leftrightarrow Li_xSn \qquad (4)$$

$$xLi^+ + C(graphene) + xe^- \leftrightarrow Li_xC \qquad (5)$$

Figure 5 (c) ∼ (f) present typical discharge and charge profiles of the SnO_2/graphene composite at different current densities of 300, 500,

700 and 1000 mA g⁻¹, with a voltage range of 3.0 ∼ 0.01 V. As shown in figure 5 (c), the initial discharge and charge capacities at a current density of 300 mA g⁻¹ are 1940 and 1224 mA h g⁻¹, respectively. When the current density increases to 500 and 700 mA g⁻¹, the discharge/charge capacities are 1810/1133 and 1660/1003 mA h g⁻¹, respectively, as shown in figure 5 (d) and (e). Even at a current density of 1000 mA g⁻¹, the initial discharge and charge capacities are 1502 and 876 mA h g⁻¹, as shown in figure 5 (f). The coulomb efficiencies of the first cycle are 63.09, 62.60, 60.42 and 58.32%, and all the coulomb efficiencies increased above 98% after 6 cycles. These values indicates that the SnO_2/graphene composite can exhibit superior lithium storage properties and that the lithium insertion and extraction reactions are highly reversible.

Figure 6 shows the cycling performance and rate performance of the SnO_2/graphene. The discharge specific capacity at a current of 100 mA g⁻¹ is 1359 mA h g⁻¹ after 100 cycles. We can see from figure 6 (a) that the discharge specific capacities are still as high as 1228, 1090, 1005 and 790 mA h g⁻¹ at current densities of 300, 500, 700 and 1000 mA g⁻¹ after 100 cycles, respectively. However, the discharge specific capacity of bare SnO_2 significantly decreases. In addition, the capacities of the composite are higher than the theoretical specific capacities of SnO_2 (782 mA h g⁻¹) and graphene (744 mA h g⁻¹), and all the discharge specific capacities at different current densities begin to increase after the 19th cycle. In order to examine the rate performance of SnO_2/graphene electrode towards different current densities, the SnO_2/graphene electrode was cycled at different current densities (300, 500, 700, 1000 mA g⁻¹) after 100 cycles at 100 mA g⁻¹, and reversed back to low current density of 100 mA g⁻¹. We can see from figure 6 (b) that the capacity decreases with increasing current densities. When the current density was reversed back to 100 mA g⁻¹, the capacity almost recover to the original value. This indicates that the SnO_2/graphene is quite suitable
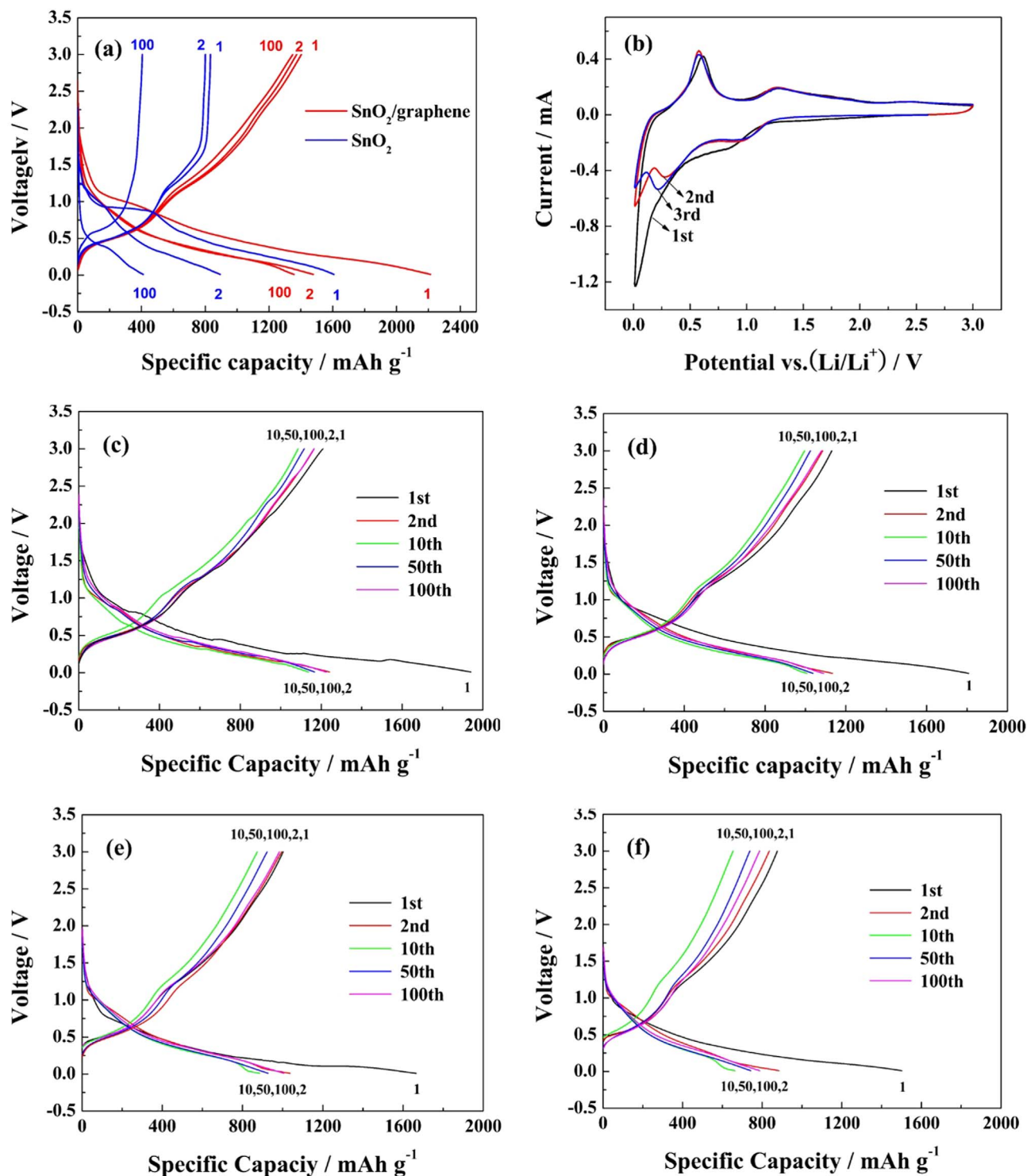
Figure 5 | Discharge/charge profiles and CV curves. (a) Discharge/charge profiles of SnO_2 and SnO_2/graphene at a current density of 100 mA g^{-1}, and (b) CV curves of SnO_2/graphene at a scanning rate of 0.1 mV s^{-1}, (c) Discharge/charge profiles of SnO_2/graphene at 300 mA g^{-1}, (b) at 500 mA g^{-1}, (c) at 700 mA g^{-1}, and (d) at 1000 mA g^{-1}.

for large current charge and discharge. The cycling performance and coulomb efficiency of SnO_2/graphene at 1000 mA g^{-1} are shown in figure 6 (c) and (d). The discharge specific capacity at the current density of 100 mA g^{-1} is 778 mA h g^{-1} after 100 cycles. The first coulomb efficiency is 58.3%, and then $\sim$ 99.5% in the following cycles. It should be noted that the capacity increases with increasing cycles of discharge and charge until 1057 mA h g^{-1} at 420th cycling, and then decreases gradually. The discharge specific capacity is stability and remains 677 mA h g^{-1} after 1000 cycles.

Figure 7 shows electrochemical impedance spectroscopy (EIS) for SnO_2/graphene before and after 1, 2, 10, 50, 100 charge/discharge cycles. The high-frequency semicircle is attributed to the constant phase element of the SEI film and contact resistance. The semicircle in the medium-frequency region is assigned to charge-transfer impedance and the constant phase element of the electrode/electrolyte interface. The inclined line is associated with Warburg impedance corresponding to the lithium-diffusion process. The diameters of the semicircles in both high and medium frequency areas become
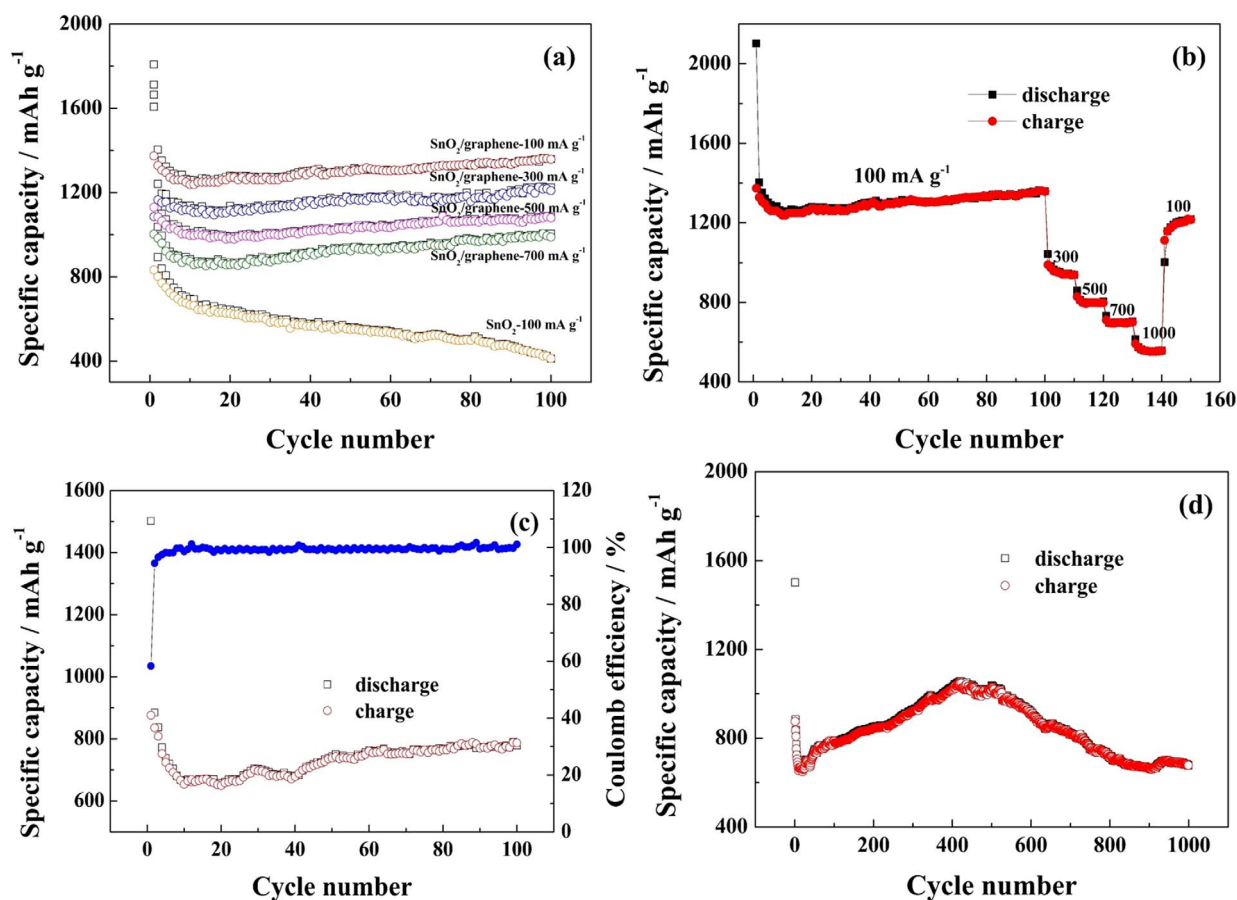
Figure 6 | Cycling performances and rate performances. (a) Cycling performance of SnO_2/graphene between 3.0 and 0.01 V at different current densities of 100, 300, 500, 700 mA g^{-1}, (b) Rate performance of SnO_2/graphene, (c) Cycling performances and coulomb efficiency at 1000 mA g^{-1} in 100 cycles, and (d) Cycling performances at 1000 mA g^{-1} in 1000 cycles.

noticeably smaller evidently after one cycle, indicating that the first several cycles are the electrode activation process and the decrease in the impedance value of SnO_2/graphene electrode. The resistances of SnO_2/graphene decrease gradually due to the size of Sn nanoparticles decrease gradually after 10, 50 and 100 cycles. The decreased resistance can enhance ionic conductivity in the composite, which is beneficial for Li$^+$ insertion/extraction into the anodes[23,30,46–47].

Figure 7 | EIS of SnO_2/graphene before and after 1, 2, 10, 50, 100 charge/discharge cycles.

Discussion

The reversible capacities only decrease in the first 19 cycles and then exhibit a slight increase with additional discharge/charge. The decay of reversible capacities of the SnO_2/graphene during the first 19 cycles can be attributed to the pulverization of original SnO_2 and in situ formed Sn nanoparticles during Li insertion and extraction process, which lead to loss of electrical connectivity between neighboring particles[12]. In the initial cycles, the pulverized particles did not contact well with each other, as a result, the reversible specific capacity decreases. However, the Sn nanoparticles began shrink and pulverize into small particles when Li$^+$ was extracted. With Li insertion and extraction, the formed Sn nanoparticles became smaller and smaller due to electrochemical milling effects and strong attached to the graphene sheets. Therefore, the conversion reaction of SnO_2 in the SnO_2/graphene composite, $SnO_2 + 4Li^+ + 4e^- \rightarrow 2Li_2O + Sn$, would be reversible to a certain extent due to the very small Sn nanoparticles. Ahn *et al.* claimed that the decrease of reagent particle size could reduce the activation energy for solid-state double decomposition reaction, thus boosting the conversation reaction and contributing to the reversible capacity[48].

The cycling performances are almost superior to most SnO_2/graphene composites, especially at high current densities. The excellent reversible capacities are also attributed to the critical size of SnO_2 nanoparticles[49]. It is reported that the particle size is one of the key factors for the stable cycling performance of SnO_2, where smaller particle size can help to prevent gradual aggregation of Sn into large clusters[50]. Kim et al. proved that particles with larger sizes are more vulnerable to aggregating into tetragonal Sn clusters, whereas ∼ 3 nm sized SnO_2 shows no aggregation upon cycling with cubic Sn
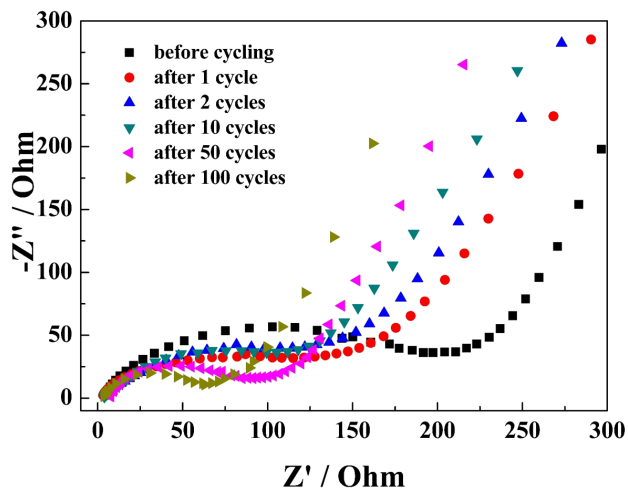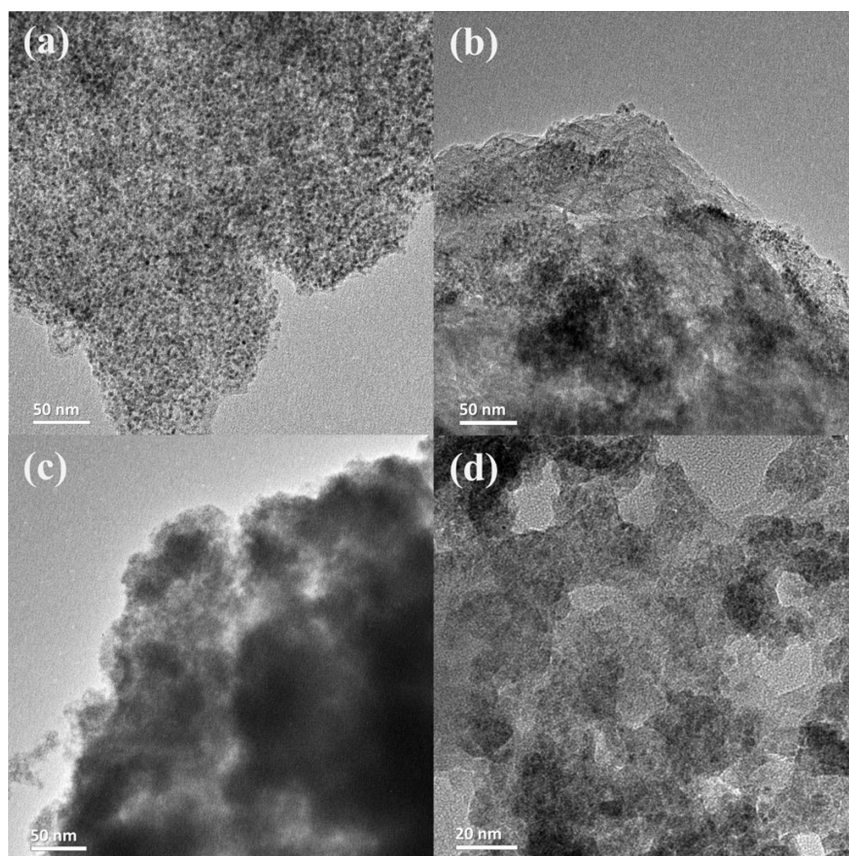
Figure 8 | TEM images of SnO$_2$/graphene composite after different discharge/charge cycles at a current density of 1000 mA g^{-1}. (a) After 20 charge/discharge cycles, (b) After 100 charge/discharge cycles, (c) After 400 charge/discharge cycles, and (d) After 1000 charge/discharge cycles.

formation[51]. In order to explore the root of the excellent cycling stability and high capacity of the SnO$_2$/graphene composite, the morphologies of electrode materials after cycling performance testing were studied. Figure 8 shows the TEM images of SnO$_2$/graphene composite after 15, 100, 400 and 1000 cycles of discharge/charge test at 1000 mA g^{-1}. As can be seen from figure 8 (a), SnO$_2$ nanoparticles are uniformly distributed on the graphene sheets, indicating that SnO$_2$/graphene composite can maintain its structure after 15 cycles. After 100 cycles, the average size of nanoparticles become small, but the boundaries of SnO$_2$ nanoparticles are still clear (figure 8 (b)). After 400 cycles, the nanoparticles no longer show clear boundaries because of repeated lithium alloying and dealloying (figure 9 (c)). But the capacity of SnO$_2$/graphene composite in the 400th cycle shows no fade, which is similar with reported in literatures[52–54]. All these phenomena reveal that the interaction between SnO$_2$ nanoparticles and graphene sheets is very strong before 400 cycles of discharge/charge test at 1000 mA g^{-1}, and reversible reaction of SnO$_2$ in the SnO$_2$/graphene composite is more and more thoroughly due to the size of nanoparticles become smaller and smaller. Therefore, the specific capacity of SnO$_2$/graphene increases during the first 400 cycles in cycling performances measurement at 1000 mA g^{-1}. Figure 8 (d) shows the TEM images of SnO$_2$/graphene composite after 1000 cycles. The size of SnO$_2$ nanoparticles become large and the surface of the nanosheets becomes textured and big holes, indicating the SnO$_2$ nanoparticles begin peeling off after long cycles due to the large volume changes. As a result, the specific capacity gradually decreases after 420th cycling. But it is worth noting that the reversible capacity of SnO$_2$/graphene composite is stability at last. Chen *et al.* reported that the porous nanostructure have more edges, which were able to provide more activated sites for Li storage and also facilitated the penetration of the electrolytes[49]. Fan *et al.* claimed that the theoretical reversible capacity for porous graphene with more edges for Li stor-

age could reach as high as 1965 mA h g^{-1}[55]. Therefore, such excellent cycling performances may be related to the porous network structure of the SnO$_2$/graphene composite. The porous structure can facilitate liquid electrolyte diffusion into the electrode material. Meanwhile, SnO$_2$ nanoparticles in the as-prepared SnO$_2$/graphene composite can reduce the path length for Li$^+$ transport and the porous graphene sheets can increase theoretical lithium storage capacity. Therefore, although the structure of SnO$_2$/graphene composite have changed after prolonged cycling process, the reversible capacity of SnO$_2$/graphene composite is stability and remains 677 mA h g^{-1} after 1000 cycles at the large current density of 1000 mA g^{-1}.

In summary, a SnO$_2$/graphene composite has been synthesized successfully by a one-step microwave-hydrothermal method. This method features quick heating, easily controlled pressure and temperature, high yield rate, and good homogeneity. In the reaction process, liquid graphite oxide as a precursor material is reduced more fully in situ, and bivalent tin ion is oxidized under microwave and high pressure with the assistance of bivalent tin and without auxiliary reagents. SnO$_2$ nanoparticles of $\sim$ 3 nm distributes on the graphene uniformly and formed nanoporous composites with large numbers of void spaces. The uniform composite shows high specific capacity and excellent cycling stability performance for LIBs at high current densities. The superior Li+ storage performances of SnO$_2$/graphene composite as anode materials for LIBs are attributed to the following benefits. (1) The critical size of SnO$_2$ nanoparticles ensures the isolation of nanoparticles with cubic Sn formation and is beneficial for the suppression of their aggregation during electrochemical discharge/charge process, resulting in improved cycling stability. (2) The uniform SnO$_2$ nanoparticles in the as-prepared SnO$_2$/graphene composite can reduce the path length for Li$^+$ transport and supply large specific surface, which is suitable for large current density charge and discharge. (3) The strong contact between SnO$_2$ nanoparticles and

graphene sheets can guarantee the stability of the SnO_2/graphene composite, which can suppress peel off of SnO_2 nanoparticles and increase the electronic conductivity. (4) The porous network structure of the SnO_2/graphene composite can increase theoretical lithium storage capacity and abundant active sites for full utilization of active materials, also can facilitate liquid electrolyte diffusion into the electrode material, which is beneficial for achieve high reversible capacity. The results of electrochemical measurement show that the SnO_2/graphene composite synthesized by the one-step microwave-hydrothermal method is a promising anode material for LIBs.

Methods

Preparation of graphite oxide and graphene oxide. Graphene oxide solution was synthesized by a modification to Hummer's method. Briefly, 2 g expanded graphite was added to a 500 mL beaker, followed by 150 mL concentrated sulfuric acid; the beaker was then placed in an ice-water bath and stirred for 10 min. Potassium permanganate (8 g) was added slowly and stirred for 30 min, then the beaker was placed in a water bath at 35°C and stirred with a mechanical stirrer for 24 h. Deionized water (100 mL) was added to the beaker at 98°C and stirred for 10 min. Then 40 mL H_2O_2 (30%) was added to the mixture and continuously stirred for 1 h. The mixture was filtered and washed with 10% HCl and 1% H_2O_2 solutions until the pH was 5. Graphite oxide of 1 mg mL^{-1} as a precursor material was exfoliated by high power ultrasonication for 30 min.

Preparation of SnO_2/graphene composite. The SnO_2/graphene composite was prepared by a one-step microwave-hydrothermal method. In a typical reaction, 35 mL 0.04 mol L^{-1} $SnCl_2 \cdot 2H_2O$ solution (0.3159 g $SnCl_2 \cdot 2H_2O$ and 35 mL deionized water) was added to 120 mL 1 mg mL^{-1} graphene oxide aqueous solution, followed by ultrasonic treatment for 10 min. The brown supernatant solution was transferred to high pressure Teflon vessels of the microwave reaction system (Anton Paar Synthos 3000). The system power, temperature, pressure and reaction time were 1000 W, 200°C, 20 bar and 30 min, respectively. The black as-synthesized product was cleaned several times by centrifugation with ethanol and deionized water.

Preparation of SnO_2 nanoparticles and graphene sheets. As comparison, graphene sheets were prepared with a one-step microwave-hydrothermal method under the same parameters without the addition of $SnCl_2 \cdot 2H_2O$. Pure SnO_2 was prepared by a microwave-hydrothermal method, then 15 mL polyethylene glycol (MW = 400) was added to 30 mL $SnCl_4 \cdot 5H_2O$ solution with concentration of 0.04 mol L^{-1}; the pH was adjusted by ammonia. The autoclave was sealed and placed in a microwave reaction system at 200°C for 60 min. The hoary solid product was annealed under 500°C for 2 h.

Sample characterization. The structure and morphology of the as-prepared materials were characterized by SEM (QUANTA 200F), TEM (FEI TECNAI G2 F20), TGA (HITACHI, STA7300), and XRD (Bruker D8 Advance with Cu Kα radiation) operated at 40 kV and 40 mA. Raman (Renishaw RM-1000) were recorded in a plus laser Raman spectrometer with an excitation laser beam wavelength of 514.5 nm. FT-IR analysis was carried out using pressed KBr disks in the range 4000–400 cm^{-1} with a PerkinElmer spectrometer. XPS (VG Scientific ESCALAB 2201XL) was carried out using Al Kα X-ray radiation and fixed analyzer transmission mode.

Electrochemical measurements. Electrochemical measurements were carried out using CR2025 coin-type cells. The working electrode was prepared by coating slurries consisting of the active material, polyvinylidene fluoride and acetylene black with a weight ratio of 80 : 10 : 10 in N-methyl-pyrrolidone solvent. The slurries were uniformly pasted on a copper foil thin film and dried at 120°C in a vacuum oven for 12 h. The thin film on copper foil was cut into round disks with diameter of 12 mm and pressed under a pressure of approximately 200 kg cm^{-2}. The films were then dried at 120°C in a vacuum oven for 3 h and used as anodes for the coin cells. The weight of working electrode materials is ~ 1.15 mg, and the weight of SnO_2/graphene composite in a coin cell for testing is 0.9124 mg. The coin cells were assembled inside a glove box filled with pure argon, using lithium metal as the counter/reference electrode and Celgard2325 as the separator. The electrolyte was 1 M LiPF$_6$ dissolved in a mixture of dimethyl carbonate, diethyl carbonate and ethylene carbonate (1 : 1 : 1 by weight). Galvanostatic charge-discharge curves of the cells were recorded by a Battery Testing System (Neware Electronic Co., China) at various current densities from 100 to 1000 mA h g^{-1} with the voltage between 3.0 and 0.01 V *versus* Li$^+$/Li at room temperature. CV curves were measured from 0.01 to 3.0 V at a scanning rate of 0.1 mV s^{-1}, and EIS data were obtained by applying an AC voltage of 5 mV in the frequency range of 0.01–100 kHz using an electrochemistry working station (AUTOLAB PGSTAT302).

1. Geim, A. K. & Novoselov, K. S. The rise of graphene. *Nat. Mater.* **6**, 183–191 (2007).
2. Geim, A. K. Graphene: Status and Prospects. *Nature.* **324**, 1530–1534 (2009).
3. Mai, Y. J. *et al.* CuO/graphene composite as anode materials for lithium-ion batteries. *Electrochem Acta.* **56**, 2306–2311 (2011).
4. Zhang, Y., Wang, X., Zeng, L., Song, S. & Liu, D. Green and controlled synthesis of Cu_2O-graphene hierarchical nanohybrids as high-performance anode materials for lithium-ion batteries via an ultrasound assisted approach. *Dalton Trans.* **41**, 4316–4319 (2012).
5. Peng, C. *et al.* Facile Ultrasonic Synthesis of CoO Quantum Dot/Graphene Nanosheet Composites with High Lithium Storage Capacity. *ACS Nano.* **6**, 1074–1081 (2012).
6. Wu, Z. *et al.* Graphene Anchored with Co_3O_4 Nanoparticles as Anode of Lithium Ion Batteries with Enhanced Reversible Capacity and Cyclic Performance. *ACS Nano.* **4**, 3187–3196 (2010).
7. Wang, G. *et al.* Preparation of Fe_2O_3/graphene composite and its electrochemical performance as an anode material for lithium ion batteries. *Journal of Alloys and Compounds.* **509**, L216–L220 (2011).
8. Zhou, G. *et al.* Graphene-Wrapped Fe_3O_4 Anode Material with Improved Reversible Capacity and Cyclic Stability for Lithium Ion Batteries. *Chem. Mater.* **22**, 5306–5313 (2010).
9. Kim, I. T., Magasinki, A., Jacob, K., Yushin, G. & Tannenbaum, R. Synthesis and electrochemical performance of reduced graphene oxide/maghemite composite anode for lithium ion batteries. *Carbon.* **52**, 56–64 (2013).
10. Wang, B., Park, J., Wang, C., Ahn, H. & Wang, G. Mn_3O_4 nanoparticles embedded into graphene nanosheets: Preparation, characterization, and electrochemical properties for supercapacitors. *Electrochim Acta.* **55**, 6812–6817 (2011).
11. Kottegoda, I. R. M., Idris, N. H., Lu, L., Wang, J. & Liu, H. Synthesis and characterization of graphene-nickel oxide nanostructures for fast charge-discharge application. *Electrochim Acta.* **56**, 5815–5822 (2011).
12. Lian, P. *et al.* High reversible capacity of SnO_2/graphene nanocomposite as an anode material for lithium-ion batteries. *Electrochim Acta.* **56**, 4532–4539 (2011).
13. Hu, T. *et al.* Flexible free-standing graphene-TiO_2 hybrid paper for use as lithium ion battery anode materials. *Carbon.* **51**, 322–326 (2013).
14. Yao, J., Shen, X., Wang, B., Liu, H. & Wang, G. In situ chemical synthesis of SnO_2-graphene nanocomposite as anode materials for lithium-ion batteries. *Electrochem. Commun.* **11**, 1849–1852 (2009).
15. Nethravathia, C., Viswanathb, B., Michaela, J. & Rajamatha, M. Hydrothermal synthesis of a monoclinic VO_2 nanotube-graphene hybrid for use as cathode material in lithium ion batteries. *Carbon.* **50**, 4839–4846 (2013).
16. Yan, M. *et al.* Nanowire Templated Semihollow Bicontinuous Graphene Scrolls: Designed Construction, Mechanism, and Enhanced Energy Storage Performance. *J. Am. Chem. Soc.* **135**, 18176–18182 (2013).
17. Chen, T., Pan, L., Liu, X., Yu, K. & Sun, Z. One-step synthesis of SnO_2-reduced graphene oxide-carbon nanotube composites via microwave assistance for lithium ion batteries. *RSC Adv.* **2**, 11719–11724 (2012).
18. Yang, A. *et al.* A simple one-pot synthesis of graphene nanosheet/SnO_2 nanoparticle hybrid nanocomposites and their application for selective and sensitive electrochemical detection of dopamine. *J. Mater. Chem. B.* **1**, 1804–1811 (2013).
19. Park, S. *et al.* A facile hydrazine-assisted hydrothermal method for the deposition of monodisperse SnO_2 nanoparticles onto graphene for lithium ion batteries. *J. Mater. Chem.* **22**, 2520–2525 (2012).
20. Zhong, C., Wang, J., Chen, Z. & Liu, H. SnO_2-Graphene Composite Synthesized via an Ultrafast and Environmentally Friendly Microwave Autoclave Method and Its Use as a Superior Anode for Lithium-Ion Batteries. *J. Phys. Chem. C.* **115**, 25115–25120 (2011).
21. Xu, W. *et al.* Heterogeneous branched core-shell SnO_2-PANI nanorod arrays with mechanical integrity and three dimentional electron transport for lithium batteries. *Nano Energy.* **8**, 196–204 (2014).
22. Zhao, B. *et al.* Bivalent tin ion assisted reduction for preparing graphene/SnO_2 composite with good cyclic performance and lithium storage capacity. *Electrochem Acta.* **56**, 7340–7346 (2011).
23. Zhu, X., Zhu, Y., Murali, S., stoller, M. & Ruoff, R. Reduced graphene oxide/tin oxide composite as an enhanced anode material for lithium ion batteries prepared by homogenous coprecipitation. *J. Power Sources.* **196**, 6473–6477 (2011).
24. Liu, H. *et al.* Flower-like SnO_2/graphene composite for high-capacity lithium storage. *Applied Surface Science.* **258**, 4917–4921 (2012).
25. Liu, H. *et al.* Hydrothermal synthesis and characterization of graphene/self-assembled SnO_2 hybrid. *Physica E.* **44**, 1931–1935 (2012).
26. Liu, H., Huang, J., Li, X., Liu, J. & Zhang, Y. SnO_2 nanorods grown on graphite as a high-capacity anode material for lithium ion batteries. *Ceramics International.* **38**, 5145–5149 (2012).
27. Zhou, X., Yin, Y., Wan, L. & Guo, Y. A robust composite of SnO_2 hollow nanospheres enwrapped by graphene as a high-capacity anode material for lithium-ion batteries. *J. Mater. Chem.* **22**, 17456–17459 (2012).
28. Zhang, J. *et al.* A simple one-pot strategy for the synthesis of ternary reduced graphite oxide/SnO_2/Au hybrid nanomaterials. *Carbon.* **49**, 3538–3543 (2011).
29. Zhang, B., Zheng, Q., Huang, Z., Oh, S. W. & Kim, J. K. SnO_2-graphene-carbon nanotube mixture for anode material with improved rate capacities. *Carbon.* **49**, 4524–4534 (2011).
30. Yang, Y. *et al.* Composites of chemically-reduced graphene oxide sheets and carbon nanospheres with three-dimensional network structure as anode materials for lithium ion batteries. *J. Mater. Chem.* **22**, 23194–23200 (2012).
31. Pan, D. *et al.* Li Storage Properties of Disordered Graphene Nanosheets. *Chem. Mater.* **21**, 3136–3142 (2009).

32. Du, Z. *et al.* In situ synthesis of SnO$_2$/graphene nanocomposite and their application as anode material for lithium ion battery. *Mater. Lett.* **64**, 2076–2079 (2010).

33. Wang, H., Robinson, J., Li, X. & Dai, H. Solvothermal Reduction of Chemically Exfoliated Graphene Sheets. *J. Am. Chem. Soc.* **131**, 9910–9911 (2009).

34. Ferrari, A. C. & Roberson, J. Interpretation of Raman spectra of disordered and amorphous carbon. *J. Phys. Rev. B.* **61**, 14095–14107 (2000).

35. Wang, Y., Chou, S., Liu, H. & Dou, S. Reduced graphene oxide with superior cycling stability and rate capability for sodium storage. *Carbon.* **57**, 202–208 (2013).

36. Zhang, L. S. *et al.* Mono dispersed SnO$_2$ nanoparticles on both sides of single layer graphene sheets as anode materials in Li-ion batteries. *J. Mater. Chem.* **20**, 5462–5467 (2010).

37. Wang, Y., Lee, J. Y. & Zeng, H. Polycrystalline SnO$_2$ Nanotubes Prepared via Infiltration Casting of Nanocrystallites and Their Electrochemical Application. *Chem. Mater.* **17**, 3899–3903 (2005).

38. Jiang, S. *et al.* Graphene-encapsulated mesoporous SnO$_2$ composites as high performance anodes for lithium-ion batteries. *J. Mater. Sci.* **48**, 3870–3876 (2013).

39. Wang, D. *et al.* Defect-Rich Crystalline SnO$_2$ Immobilized on Graphene Nanosheets with Enhanced Cycle Performance for Li Ion Batteries. *J. Phys. Chem. C.* **116**, 22149–22156 (2012).

40. Zhang, C. *et al.* Carbon-coated SnO$_2$/graphene nanosheets as highly reversible anode materials for lithium ion batteries. *Carbon.* **50**, 1897–1903 (2012).

41. Demazeau, G. Solvothermal processes: a route to the stabilization of new materials. *J. Mater. Chem.* **9**, 15–18 (1999).

42. Kong, J. *et al.* Highly electrically conductive layered carbon derived from polydopamine and its functions in SnO$_2$-based lithium ion battery anodes. *Chem. Commun.* **48**, 10316–10318 (2012).

43. Zhang, M. *et al.* Fast synthesis of SnO$_2$/graphene composites by reducing graphene oxide with stannous ions. *J. Mater. Chem.* **21**, 1673–1676 (2011).

44. Xu, C., Sun, J. & Gao, L. Controllable synthesis of monodisperse ultrathin SnO$_2$ nanorods on nitrogen-doped graphene and its ultrahigh lithium storage properties. *Nanoscale.* **4**, 5425–5430 (2012).

45. Wang, X., Zhou, X., Yao, K., Zhang, J. & Liu, Z. A SnO$_2$/graphene composite as a high stability electrode for lithium ion batteries. *Carbon.* **49**, 133–139 (2011).

46. Chen, S., Wang, Y., Ahn, H. & Wang, G. Microwave hydrothermal synthesis of high performance tin-graphene nanocomposites for lithium ion batteries. *J. Power Sources.* **216**, 22–27 (2012).

47. Su, Y. *et al.* Two-Dimensional Carbon-Coated Graphene/Metal Oxide Hybrids for Enhanced Lithium Storage. *ACS Nano.* **6**, 8349–8356 (2012).

48. Ahn, D. *et al.* Applying functionalized carbon nanotubes to enhance electrochemical performances of tin oxide composite electrodes for Li-ion battery. *J. Power Sources.* **212**, 66–72 (2012).

49. Chen, Y., Song, B., Chen, R. M., Lu, L. & Xue, J. A study of the superior electrochemical performance of 3 nm SnO$_2$ nanoparicles supported by graphene. *J. Mater. Chem. A.* **2**, 5688–5695 (2014).

50. Courtney, I. A. & Dahn, J. R. Key factors controlling the reversibility of the reaction of lithium with SnO$_2$ and Sn$_2$BPO$_6$ glass. *J. Electrochem. Soc.* **144**, 2943–2958 (1997).

51. Kim, C., Noh, M., Choi, M., Cho, J. & Park, B. Critical size of a nano SnO$_2$ electrode for Li-secondary battery. *Chem. Mater.* **17**, 3297–3301 (2005).

52. Guo, J., Jiang, B., Zhang, X. & Liu H. Monodisperse SnO$_2$ anchored reduced graphene oxide nanocomposites as negative electrode with high rate capability and long cyclability for lithium-ion batteries. *J. Power Sources.* **262**, 15–22 (2014).

53. Zhou, X. *et al.* Tin Dioxide@Carbon Core-shell Nanoarchitectures Anchored on Wrinkled Graphene for Ultrafast and Stable Lithium Storage. *ACS Appl. Mater. Interfaces.* **6**, 7434–7443 (2014).

54. Li, N., Song, H., Cui, H. & Wang C. SnO$_2$ nanoparticles anchored on vertically aligned graphene with a high rate, high capacity, and long life for lithium storage. *Electrochim. Acta.* **130**, 670–678 (2014).

55. Fan, Z. *et al.* Porous graphene netwoks as high performance anode materials for lithium ion batteries. *Carbon.* **60**, 558–561 (2013).

Author contributions

M.Z.A. originated the work and designed the experiments. L.L.L. performed the experiments, analyzed the data and wrote the manuscript. P.X.Y. performed XPS and XRD measurement and data analysis. J.Q.Z. carried out cyclic voltammetry and electrochemical impedance spectroscopy measurement and data analysis. All authors reviewed the manuscript.

Additional information

How to cite this article: Liu, L., An, M., Yang, P. & Zhang, J. Superior cycle performance and high reversible capacity of SnO$_2$/graphene composite as an anode material for lithium-ion batteries. *Sci. Rep.* **5**, 9055; DOI:10.1038/srep09055 (2015).